

Cosmic archaeology with massive stellar black hole binaries

L. Graziani^{1,2,3} ^{*}, R. Schneider^{1,2,4}, S. Marassi^{1,2}, W. Del Pozzo⁵, M. Mapelli^{6,7,8},
N. Giacobbo^{6,7,8}

¹*Dipartimento di Fisica, Sapienza, Università di Roma, Piazzale Aldo Moro 5, 00185, Roma, Italy*

²*INFN, Sezione di Roma I, P.le Aldo Moro 2, 00185 Roma, Italy*

³*INAF/Osservatorio Astrofisico di Arcetri, Largo E. Fermi 5, 50125 Firenze, Italy*

⁴*INAF/Osservatorio Astronomico di Roma, Via di Frascati 33, 00078 Monte Porzio Catone, Italy*

⁵*Dipartimento di Fisica “Enrico Fermi”, Università di Pisa, Pisa I-56127, Italy*

⁶*Dipartimento di Fisica e Astronomia “G. Galilei”, Università di Padova, vicolo dell’Osservatorio 3, 35122 PD, Italy*

⁷*INFN, Sezione di Padova, Via Marzolo 8, I-35131 Padova, Italy*

⁸*INAF/Osservatorio Astronomico di Padova, Vicolo dell’ Osservatorio 5, I-35122, Padova, Italy*

Accepted XX <Month> XX. Received 2019 <Month> XX; in original form 2019 <Month> XX

ABSTRACT

The existence of massive stellar black hole binaries (MBHBs), with primary black hole (BH) masses $\geq 31 M_{\odot}$, was proven by the detection of the gravitational wave (GW) event GW150914 during the first LIGO/Virgo observing run (O1), and successively confirmed by seven additional GW signals discovered in the O1 and O2 data. By adopting the galaxy formation model **GAMESH** coupled with binary population synthesis (BPS) calculations, here we investigate the origin of these MBHBs by selecting simulated binaries compatible in mass and coalescence redshifts. We find that their cosmic birth rates peak in the redshift range $6.5 \leq z \leq 10$, regardless of the adopted BPS. These MBHBs are then old systems forming in low-metallicity ($Z \sim [0.01 - 0.1] Z_{\odot}$), low-stellar-mass galaxies, before the end of cosmic reionization, i.e. significantly beyond the peak of cosmic star formation. GW signals generated by coalescing MBHBs open up new possibilities to probe the nature of stellar populations in remote galaxies, at present too faint to be detected by available electromagnetic facilities.

Key words: Cosmology: theory - Cosmic UV background - IGM - metal ions

1 INTRODUCTION

Since the discovery of the first GW signal GW150914 (Abbott et al. 2016) and to date, the LIGO/Virgo Collaboration detected four events interpreted as originated by the coalescence of MBHBs (i.e. systems with $m_1 \in [31, 66] M_{\odot}$, $m_2 \in [21, 43] M_{\odot}$) at a median luminosity distance $d_L \geq 440$ Gpc (Abbott et al. 2019a); interestingly enough, a recent independent data analysis (Venumadhav et al. 2019) expanded the above sample with four new systems (see Table 1). Even more intriguing, the current O3 run has already reported more than fourteen alerts with similarly high d_L ¹.

Future ground-based interferometers, such as KAGRA (Akutsu et al. 2019) and LIGO-India will join the global GW detector network improving the event localization up to 90%-confidence (Abbott et al. 2018). Space-based missions will target the milli-Hz band with LISA² and the deci-Hz

band with DECIGO³. This synergistic multi-band approach (Sesana 2016) will place better constraints on MBHBs, also accessing their early inspiral phases (Isoyama et al. 2018). Finally, 3G detectors, such as the Einstein Telescope⁴ and Cosmic Explorer⁵ could detect stellar MBHBs up to extremely high redshifts (Kalogera et al. 2019).

Stellar models predict MBHBs to be the end products of metal-poor stars (Mapelli et al. 2009, 2010; Belczynski et al. 2010; Spera et al. 2015). Given our current understanding of galaxy evolution, these stars are preferentially formed in low-mass and less-chemically-evolved galaxies (Maiolino & Mannucci 2019), hardly resolved by large scale cosmological simulations.

BPS codes are traditionally adopted to investigate the evolution of BH binaries by generating databases (DB) from distributions of initial stellar masses and orbital param-

^{*} E-mail: luca.graziani@roma1.infn.it

¹ <https://gracedb.ligo.org/latest/>

² <https://www.elisascience.org/>

³ <http://tamago.mtk.nao.ac.jp/decigo/>

⁴ <http://www.et-gw.eu/>

⁵ <https://cosmicexplorer.org/>

	GW150914	GW170729	GW170818	GW170823	GW170304	GW170403	GW170425	GW170727
m_1/M_\odot	$35.6^{+4.8}_{-3.0}$	$50.2^{+16.2}_{-10.2}$	$35.4^{+7.5}_{-4.7}$	$39.5^{+11.2}_{-6.7}$	$41.0^{+12.0}_{-7.0}$	$44.0^{+12.0}_{-8.0}$	$44.0^{+19.0}_{-10.0}$	$39.0^{+10.0}_{-6.0}$
m_2/M_\odot	$30.6^{+3.0}_{-4.4}$	$34.0^{+9.1}_{-10.1}$	$26.7^{+4.3}_{-5.2}$	$29.4^{+6.7}_{-7.8}$	$31.0^{+7.0}_{-8.0}$	$32.0^{+8.0}_{-9.0}$	$29.0^{+11.0}_{-8.0}$	$29.0^{+6.0}_{-7.0}$
\mathcal{M}/M_\odot	$28.6^{+1.7}_{-1.5}$	$35.4^{+6.5}_{-4.8}$	$26.5^{+2.1}_{-1.7}$	$29.2^{+4.6}_{-3.6}$	$47.0^{+8.0}_{-7.0}$	$48.0^{+9.0}_{-7.0}$	$47.0^{+26.0}_{-10.0}$	$42.0^{+6.0}_{-6.0}$
M_f/M_\odot	$63.1^{+3.4}_{-3.0}$	$79.5^{+14.7}_{-10.2}$	$59.4^{+4.9}_{-3.8}$	$65.4^{+10.1}_{-7.4}$				
d_L/Mpc	440^{+150}_{-170}	2840^{+1400}_{-1360}	1060^{+420}_{-380}	1940^{+970}_{-900}				
z_c	$0.09^{+0.03}_{-0.03}$	$0.49^{+0.19}_{-0.21}$	$0.21^{+0.07}_{-0.07}$	$0.35^{+0.15}_{-0.15}$	$0.50^{+0.2}_{-0.2}$	$0.45^{+0.22}_{-0.19}$	$0.50^{+0.4}_{-0.3}$	$0.43^{+0.17}_{-0.17}$
\mathcal{R} (SeBa/MOBSE)	2.01/87.26	0.06/6.81	5.23/124.90	5.65/111.10	7.14/52.34	6.99/49.12	7.38/108.63	6.37/112.39

Table 1. Properties of the GW events (in column) associated with the MBHBs found in O1 and O2 (Abbott et al. 2019a) and extended by Venumadhav et al. (2019) (although with lower p_{astro} and FAR values, GW IDs in bold). Each row shows: source frame component masses m_1 and m_2 , chirp mass \mathcal{M} , final source frame mass M_f , luminosity distance d_L , estimated coalescence redshift z_c and estimated coalescence rates (\mathcal{R} [$\text{cGpc}^{-3} \text{ yr}^{-1}$]) predicted by SeBa/ MOBSE in our Local Group-like volume of 4^3 cMpc^3 .

ters. By coupling them with estimates of the cosmic star formation rate (SFR) and of the average metallicity evolution (or mass-metallicity relation), their coalescence rates along z can be inferred (Schneider et al. 2010; Marassi et al. 2009, 2011; Regimbau 2011; Dominik et al. 2013; Belczynski et al. 2016; Lamberts et al. 2016; Dvorkin et al. 2016; Elbert et al. 2018; Chruslinska et al. 2019; Neijssel et al. 2019; Bavera et al. 2019). With hydrodynamic simulations or semi-analytic models (SAMs) the cosmological evolution of compact binaries can be studied connecting galaxies hosting their birth and coalescence (Schneider et al. 2017; Mapelli et al. 2017; O’Shaughnessy et al. 2017; Mapelli & Giacobbo 2018; Marassi et al. 2019; Artale et al. 2019).

Here we use the GAMESH model to predict the origin of MBHBs in a Local Group-like volume. In Schneider et al. (2017) we already investigated the birth and coalescence sites of compact binaries generating O1 GW events, while in Marassi et al. (2019) we looked at observational counterparts of GW150914 hosts. Here, we go one step forward by exploring the birth and coalescence of the MBHBs in Table 1, with an increased statistical sample of massive binaries and by comparing predictions of two independent BPS databases (DB): SeBa (Portegies Zwart & Verbunt 1996; Mapelli et al. 2013) and MOBSE (Giacobbo et al. 2018).

We provide the statistical evidence that the highest birth rate of their stellar progenitors is found in low metallicity ($Z \leq 0.1 Z_\odot$), star forming, dwarf galaxies living in the redshift range $6.5 \leq z \leq 10$, i.e. in the epoch of reionization (EoR, $z \geq 6$). While this result is proven to be independent of the adopted BPS, the number of coalescence events strongly depends on the prescriptions implemented in binary evolution codes for massive BH formation.

2 GALAXY FORMATION MODEL

GAMESH (Graziani et al. 2015, 2017; Graziani 2019) is a galaxy formation model based on a hybrid pipeline combining a Dark Matter (DM)-only simulation, a SAM for star formation and chemical evolution and a radiative transfer module. The DM run simulates a multi-zoom cosmic box better resolved in its inner cubic volume of 4^3 cubic comov-

ing mega-parsecs (cMpc^3), centered on a Milky Way-like halo (a Local Group-like volume). The SAM module runs on a galaxy catalog taken from a larger volume ($\sim 8^3 \text{ cMpc}^3$) to capture a wider statistics of intermediate/dwarf galaxies whose stellar and chemical evolution in $0 < z < 20$ is regulated by two parameters: star formation and wind efficiency. The resulting baryonic properties of the MW are in agreement with observations. Moreover, the histories of a plethora of well resolved dwarf galaxies, co-evolving under strong dynamical interactions and feedback⁶, naturally reproduce observed galaxy scaling relations (Graziani et al. 2017; Ginolfi et al. 2018). In Schneider et al. (2017) GAMESH was extended to self-consistently account for compact binary systems by assigning a binary fraction of $f_{2,*} = 1$ and by randomly sampling the newly formed stellar mass with a SeBa DB having 2×10^6 binaries in the IMF mass range $M_* \in [0.01, 100] M_\odot$. Here we adopt two new independent DBs improving the statistics of MBHBs: a MOBSE DB with 10^7 binaries sampling $M_* \in [5.0, 150]$ and a SeBa DB with 2×10^7 systems in $M_* \in [8.0, 100]$. Each DB has 12 metallicity bins, regularly spanning the range $Z \in [0.01, 1] Z_\odot$ ⁷. While the two BPS assume the same stellar evolutionary tracks and metallicity dependent mass loss in stellar winds⁸, the stellar evolution channels producing massive BHs are significantly different: the MOBSE $\alpha 5$ run adopts the rapid SN model of Fryer et al. (2012), while in SeBa all stars with pre-SN masses $m_{\text{pre,SN}} \geq 40 M_\odot$ are assumed to collapse into a BH with no SN explosion; the resulting BH mass is then $m_{\text{BH}} = m_{\text{CO}} + (2/3)(m_{\text{He}} + m_{\text{H}})$ (Mapelli et al. 2013).

⁶ Here radiative feedback is implemented by assuming that the volume instantly re-ionizes at $z = 6$.

⁷ For details on the set-up of the two DBs, please refer to the $\alpha 5$ run of Giacobbo & Mapelli (2018) and to Schneider et al. (2017). We also assume $Z_\odot = 0.02$. Finally note that the prescriptions in MOBSE and SeBa are not tailored to describe systems to describe systems with $Z < 0.01 Z_\odot$ and we are forced to extrapolate the results of $Z = 0.01 Z_\odot$ at lower metallicities, with a possible impact on the results, especially for galaxies hosting Pop III stars.

⁸ In MOBSE the metallicity dependence is also suppressed when the electron scattering Eddington factor $\Gamma_e \geq 2/3$ (Giacobbo et al. 2018).

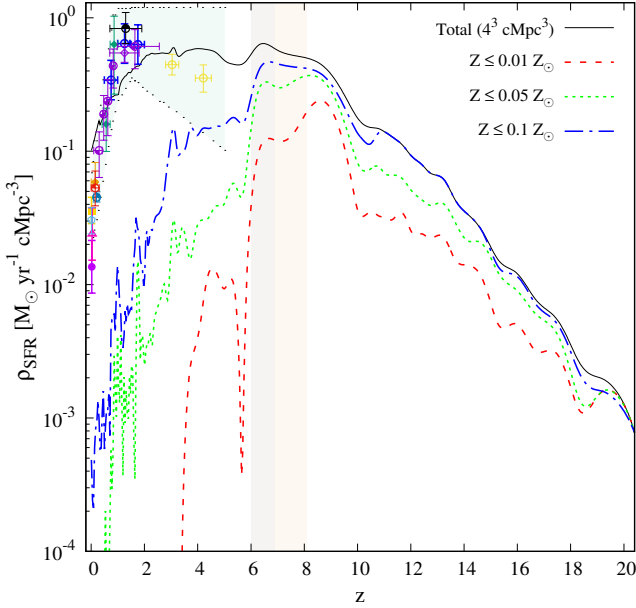


Figure 1. Star formation rate density as a function of redshift z in the $(4 \text{ cMpc})^3$ volume: total (solid black), from galaxies with $Z_{\star} \leq 0.01 Z_{\odot}$ (dashed red line), $Z_{\star} \leq 0.05 Z_{\odot}$ (dotted green), and $Z_{\star} \leq 0.1 Z_{\odot}$ in dotted-dashed blue line. Shaded areas indicate the redshift range of the reionization midpoint $6.9 < z_{50\%} < 8.1$ (light pink, Planck Collaboration et al. (2018)) and the assumed end of reionization (gray). Observational data and its general level of uncertainty in the Local Volume (cyan shaded area) are collected from Hopkins et al. (2001).

The Common Envelope (CE) efficiencies also differ: $\alpha = 1.0$, $\lambda = 0.5$ in **SeBa**, while in **MOBSE** $\alpha = 5$ and λ depends on the stellar type. Note that these parameters critically affect the statistics of low-mass BHBs but have a minor impact on the merger rate of MBHBs (Giacobbo et al. 2018).

Once the newly formed M_{\star} in each galaxy is populated with binaries randomly sampled from the DB with Z closest to the stellar metallicity Z_{\star} , we follow them in time from their birth (t_0) to coalescence (t_c), by relating ancestors with descendant galaxies. In Fig. 1 we show the predicted total SFR density ρ_{SFR} as a function of redshift (solid black line). Dashed-red, dotted-green and dashed-dotted blue lines correspond to the same quantity computed by summing up the contributions of star forming galaxies with $Z_{\star} \leq 0.01, 0.05, 0.1 Z_{\odot}$, respectively. The simulated trend is in very good agreement with the observational data at $z < 4$ and their range of uncertainty, collected from Hopkins et al. (2001). Noticeably, systems with $Z \leq 0.05 Z_{\odot}$ provide a major contribution to ρ_{SFR} from the cosmic dawn ($z \sim 18$) down to $z \sim 6$, making small, normal star forming galaxies (see Graziani et al. 2020 for a definition) the dominant population at these epochs. Gas photo-heating associated to cosmic reionization progressively diminishes their contribution (see the relative drops in red/green/blue lines) until the total SFR becomes sustained only by intermediate-mass galaxies hosted in Ly α -cooling halos at $z < 6$ (Graziani et al. 2015).

3 RESULTS

Before presenting our results, we note here that MBHBs are identified in the simulation by requiring that both masses, m_1, m_2 , and coalescence redshift z_c (derived from t_c) lie within the observational uncertainties reported in Table 1.

3.1 MBHBs formation sites and birth rates

The birth rates of stellar progenitors evolving into the selected MBHBs are shown in Fig. 2, as a function of z ; top/bottom panels show rates obtained coupling with **SeBa**/**MOBSE** with identical line styles and colours for the same GW signal. It is immediately evident that all birth rates peak in the redshift range $6.5 \leq z \leq 10$ regardless the adopted BPS, and that their shape is similar across GW signals, reflecting the underlying $\text{SFR}(z)$ trend⁹. The absolute values for each signal, on the other hand, strongly vary across BPS predictions as well as their relative height and line shapes (see also Section 3.2). The coalescence rate of each MBHB is provided in the last row of Table 1, while the total merger rates (i.e. when all binary BHs in the simulation are considered, regardless of their masses) at $z = 0.2$ and $z = 0$ are $\mathcal{R}_0 = 4195$ (1513) $\text{Gpc}^{-3} \text{ yr}^{-1}$ and $\mathcal{R}_{0.2} = 5564$ (1584) $\text{Gpc}^{-3} \text{ yr}^{-1}$ for **SeBa** (**MOBSE**); consequently our MBHBs contribute only for 7 (41)% to the total value at $z = 0$.

While a direct comparison with observationally inferred rates $[24.4 - 140.4] \text{ Gpc}^{-3} \text{ yr}^{-1}$ (Abbott et al. 2019b) is not feasible because Local Group-like volumes are generally over-dense and then not representative of larger cosmological scales¹⁰, we note that Mapelli et al. (2017) adopted the same **MOBSE** DB on the Illustris simulation (with a cubic box size of $L_{\text{box}} = 106.5 \text{ cMpc}$) finding $\mathcal{R}_0 = 155 \text{ Gpc}^{-3} \text{ yr}^{-1}$ and $\mathcal{R}_{0.2} = 228 \text{ Gpc}^{-3} \text{ yr}^{-1}$, close to the 90% credible values of Abbott et al. (2019b). However, the contribution of high- z dwarfs remains mostly undetermined in large cosmological simulations and in models that adopt observationally inferred scaling relations, such as the mass-metallicity relation and galaxy main sequence, which are not yet observed at $z \geq 6$.

3.2 Metallicity dependence

The distribution in metallicity of MBHBs stellar progenitors is shown in Fig. 3; filled (dashed) histograms show the results obtained with **SeBa** (**MOBSE**). All the stellar progenitors predicted with the **SeBa** DB form at metallicity $Z \leq 0.05 Z_{\odot}$

⁹ This result is peculiar of the selected massive binaries. A broader mass selection extending to lower BH masses would shift their birth rates closer to the SFR peak. Moreover, our previous results (Schneider et al. 2017), while based on the same cosmological run, did not have enough statistical sampling of the high-mass end of the stellar initial mass function and therefore underestimated the birth rates of GW150914-like events in low-mass, low-metallicity galaxies at high z (see Section 2). Finally, the results are also confirmed by Monte Carlo convergence tests performed with different random number chains.

¹⁰ The ρ_{SFR} shown in Fig. 1 is approximately one order of magnitude larger than the cosmic star formation rate density at $z < 4$ (Madau & Fragos 2017) and flatter at higher z .

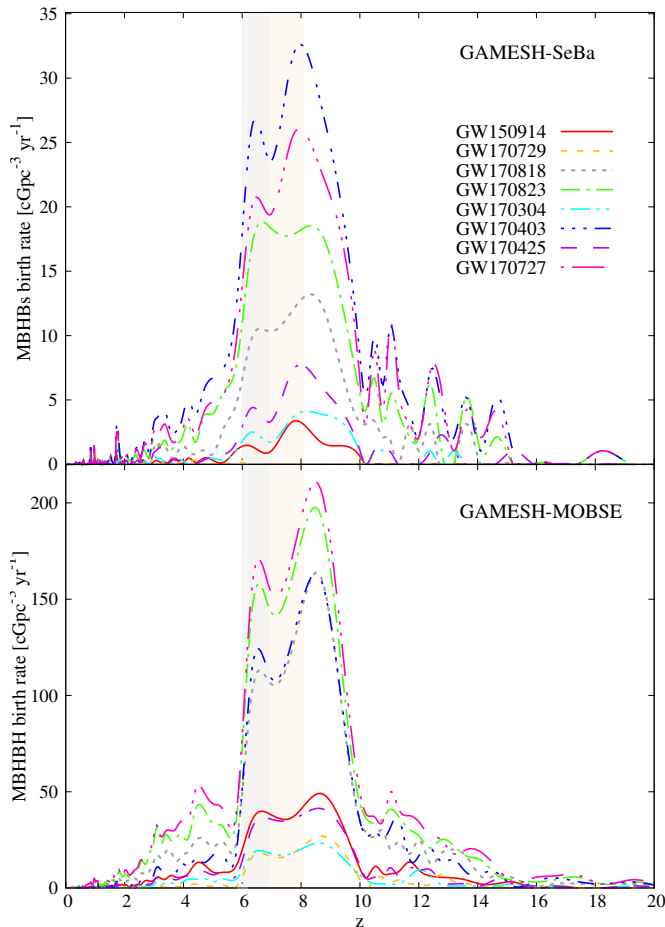


Figure 2. Birth rates [$\text{cGpc}^{-3} \text{ yr}^{-1}$] of our MBHBs stellar progenitors as a function of redshift z . The two panels adopt the same galaxy formation model but different BPS calculations: **SeBa** (top) and **MOBSE** (bottom). The light pink and gray shaded areas are the same as in Fig. 1.

following a nearly flat distribution¹¹, while **MOBSE** predictions involve higher gas metallicity, up to $Z = 0.1Z_{\odot}$. Also note that the percentage of binaries with $Z \leq 0.05Z_{\odot}$ is always higher than 66% for all the GW events. As the SFR in $6 \leq z \leq 10$ is largely dominated by galaxies with $Z \leq 0.05Z_{\odot}$ (see Fig. 1), MBHBs birth rates show the highest peak in this redshift range independently of the adopted BPS. The discrepancy in their absolute values reflect differences in the two BPS. In all metallicity bins, the number of MBHBs predicted by **MOBSE** largely exceeds the one of **SeBa**, reflecting the assumptions made on how massive BHs form. MBHBs predicted by **MOBSE** at $Z > 0.05Z_{\odot}$ also originate from very massive progenitors: GW150914-like systems with $Z \geq 0.08Z_{\odot}$, for example, have primary stars with $m_1 > 100M_{\odot}$ with sufficiently massive CO core, at the pre-SN stage, to meet the conditions of direct BH collapse, despite their mass loss (Fryer et al. 2012). Such BHs are not

¹¹ For GW170729, the most massive among the MBHB sample shown in Table 1, the number of systems predicted by **SeBa** is 32, i.e. too small to appear in the log scale adopted in 3. All these systems, however, form at $Z \leq 0.02Z_{\odot}$.

formed by **SeBa**, either because the IMF of the primary star does not extend beyond $100 M_{\odot}$ or because efficient mass loss reduces their pre-SN mass below the $40M_{\odot}$ limit, necessary for direct BH formation. Finally, it is important to stress that the histograms in Fig. 3 result from the convolution of the intrinsic BPS metallicity distribution functions and the way metallicity-dependent formation sites evolve in the cosmological simulation. Hence, these findings indicate that both BPS models predict a fraction of MBHBs to form with large orbital separations, delaying their merger by 8 - 12 Gyr since the formation.

4 CONCLUSIONS

In this paper we investigate the origin of the most massive black hole binaries ($m_1 \geq 31 M_{\odot}$) detected during the LIGO/Virgo O1 and O2 runs (see Table 1). By running the galaxy evolution model **GAMESH** coupled with **SeBa** and **MOBSE** binary population synthesis calculations, we select binaries with primary and secondary masses and coalescence redshift within the observed ranges, and establish their cosmological birth rate and the successive redshift evolution. We find that all birth rates peak in the redshift range $6.5 \leq z \leq 10$, i.e. before the end of cosmic reionization, regardless the binary population synthesis model.

Three conditions act in concert to provide this result: (i) a large number of star forming dwarf galaxies contribute the total SFR in the EoR; (ii) their chemical evolution leave the gas metallicity below $Z \approx 0.1 Z_{\odot}$; (iii) the statistics of coalescence times of MBHBs under investigation peak at very high values ($t_c > 9.5$ Gyrs) allowing them to merge in the interval of z_c inferred from the detected GW signals (Belczynski et al. 2016; Mapelli et al. 2019).

Hence, we predict these massive black hole binaries to preferentially form in low-metallicity, star forming dwarfs at redshifts significantly higher than the peak of cosmic star formation that are hardly resolved in large-scale cosmological simulations and that are beyond the observational capabilities of current electromagnetic facilities. Future gravitational wave and electromagnetic facilities will be able to improve our knowledge of these ancient systems, fully exploiting their potential as cosmic archaeology probes.

ACKNOWLEDGMENTS

LG and RS acknowledge support from the Amaldi Research Center funded by the MIUR program "Dipartimento di Eccellenza" (CUP:B81I18001170001). MM and NG acknowledge financial support by the European Research Council for the ERC Consolidator grant DEMOBLACK, under contract no. 770017.

References

- Abbott B. P., et al., 2016, *Physical Review Letters*, **116**, 061102
- Abbott B. P., et al., 2018, *Living Reviews in Relativity*, **21**, 3
- Abbott B. P., et al., 2019a, *Physical Review X*, **9**, 031040
- Abbott B. P., et al., 2019b, *ApJ*, **882**, L24
- Akutsu T., et al., 2019, *Nat. Astron.*, **3**, 35
- Artale M. C., Mapelli M., Giacobbo N., Sabha N. B., Spera M., Santoliquido F., Bressan A., 2019, *MNRAS*, **482**, 1382

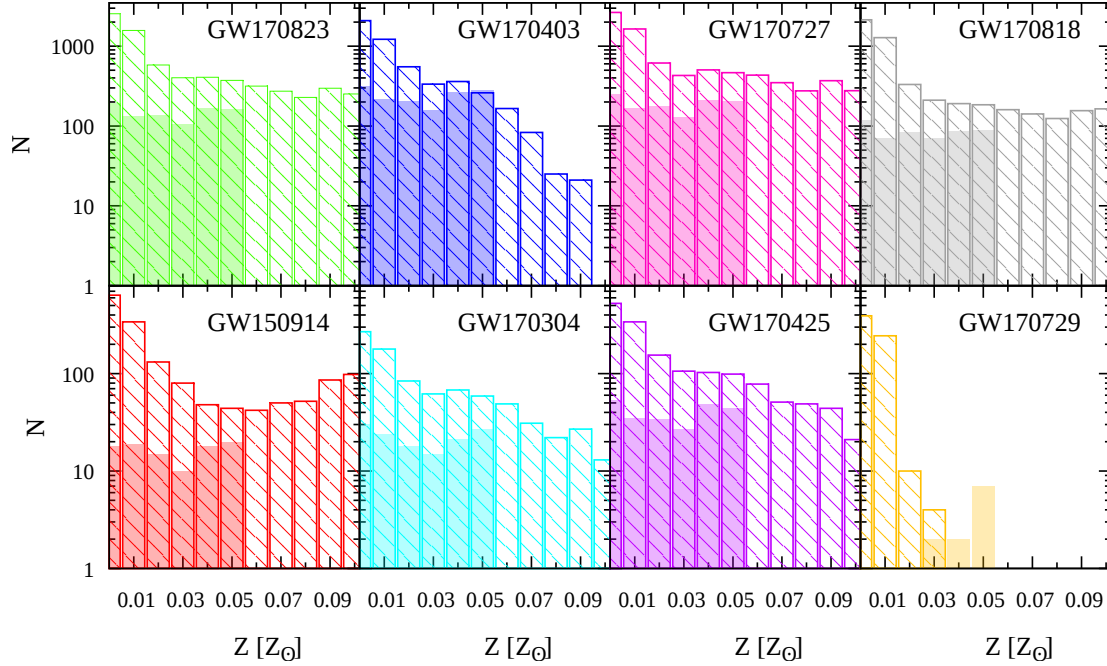


Figure 3. Total number of GW events (N , in logarithmic scale) predicted to form at each Z by **SeBa** (filled histograms) and **MOBSE** (dashed histograms) run on the same galaxy formation model. Each panel represents the results obtained for individual GW events and the colour coding is the same in Fig. 2.

Bavera S. S., et al., 2019, arXiv e-prints, p. [arXiv:1906.12257](#)
 Belczynski K., Bulik T., Fryer C. L., Ruiter A., Valsecchi F., Vink J. S., Hurley J. R., 2010, *ApJ*, **714**, 1217
 Belczynski K., Holz D. E., Bulik T., O’Shaughnessy R., 2016, *Nature*, **534**, 512
 Chruslinska M., Nelemans G., Belczynski K., 2019, *MNRAS*, **482**, 5012
 Dominik M., Belczynski K., Fryer C., Holz D. E., Berti E., Bulik T., Mandel I., O’Shaughnessy R., 2013, *Astrophysical Journal*, **779**, 72
 Dvorkin I., Vangioni E., Silk J., Uzan J.-P., Olive K. A., 2016, *mnras*, 461
 Elbert O. D., Bullock J. S., Kaplinghat M., 2018, *MNRAS*, **473**, 1186
 Fryer C. L., Belczynski K., Wiktorowicz G., Dominik M., Kalogera V., Holz D. E., 2012, *ApJ*, **749**, 91
 Giacobbo N., Mapelli M., 2018, *MNRAS*, **480**, 2011
 Giacobbo N., Mapelli M., Spera M., 2018, *MNRAS*, **474**, 2959
 Ginolfi M., Graziani L., Schneider R., Marassi S., Valiante R., Dell’Aglì F., Ventura P., Hunt L. K., 2018, *MNRAS*, **473**, 4538
 Graziani L., 2019, *Physics*, **1**, 412,429
 Graziani L., Salvadori S., Schneider R., Kawata D., de Bressan A., Maselli A., 2015, *MNRAS*, **449**, 3137
 Graziani L., de Bressan A., Schneider R., Kawata D., Salvadori S., 2017, *MNRAS*, **469**, 1101
 Graziani L., Schneider R., Ginolfi M., Hunt L. K., Maio U., Glatzle M., Ciardi B., 2020, *MNRAS*,
 Hopkins A. M., Irwin M. J., Connolly A. J., 2001, *ApJ*, **558**, L31
 Itoyama S., Nakano H., Nakamura T., 2018, *Progress of Theoretical and Experimental Physics*, **2018**, 073E01
 Kalogera V., et al., 2019, *BAAS*, **51**, 242
 Lamberts A., Garrison-Kimmel S., Clausen D. R., Hopkins P. F., 2016, *MNRAS*, **463**, L31
 Madau P., Fragos T., 2017, *ApJ*, **840**, 39
 Maiolino R., Mannucci F., 2019, *A&ARv*, **27**, 3

Mapelli M., Giacobbo N., 2018, *MNRAS*, **479**, 4391
 Mapelli M., Colpi M., Zampieri L., 2009, *MNRAS*, **395**, L71
 Mapelli M., Ripamonti E., Zampieri L., Colpi M., Bressan A., 2010, *MNRAS*, **408**, 243
 Mapelli M., Zampieri L., Ripamonti E., Bressan A., 2013, *Monthly Notices of the Royal Astronomical Society*, **429**, 2298
 Mapelli M., Giacobbo N., Ripamonti E., Spera M., 2017, *MNRAS*, **472**, 2422
 Mapelli M., Giacobbo N., Santoliquido F., Artale M. C., 2019, *J* 10.1093/mnras/stz1150
 Marassi S., Schneider R., Ferrari V., 2009, *MNRAS*, **398**, 293
 Marassi S., Schneider R., Corvino G., Ferrari V., Portegies Zwart S., 2011, *Physical Review D*, **84**, 124037
 Marassi S., Graziani L., Ginolfi M., Schneider R., Mapelli M., Spera M., Alparone M., 2019, *MNRAS*, **484**, 3219
 Neijssel C. J., et al., 2019, *MNRAS*, **490**, 3740
 O’Shaughnessy R., Bellovary J. M., Brooks A., Shen S., Governato F., Christensen C. R., 2017, *MNRAS*, **464**, 2831
 Planck Collaboration et al., 2018, arXiv e-prints, p. [arXiv:1807.06209](#)
 Portegies Zwart S. F., Verbunt F., 1996, *A&A*, **309**, 179
 Regimbau T., 2011, *Research in Astronomy and Astrophysics*, **11**, 369
 Schneider R., Marassi S., Ferrari V., 2010, *Classical and Quantum Gravity*, **27**, 194007
 Schneider R., Graziani L., Marassi S., Spera M., Mapelli M., Alparone M., de Bressan A., 2017, *MNRAS*, **471**, L105
 Sesana A., 2016, *Prl*, **116**, 231102
 Spera M., Mapelli M., Bressan A., 2015, *MNRAS*, **451**, 4086
 Venumadhav T., Zackay B., Roulet J., Dai L., Zaldarriaga M., 2019, arXiv e-prints, p. [arXiv:1904.07214](#)